DOI: 10.15669/pnst.8.165

Progress in Nuclear Science and Technology
Volume 8 (2025) pp. 165-170

ARTICLE

Validation Study on SFR Core Bowing Codes using Joyo Ex-Core Experiment Data: Multiple Duct Bowing Benchmark

Nicholas WOZNIAK [1*], Kazuya OHGAMA [2], Norihiro DODA [2], Hirokazu OHTA [3], Emily SHEMON [1], Bo FENG [1], Tomoyuki UWABA [2], Satoshi FUTAGAMI [2], Masaaki TANAKA [2], Hidemasa YAMANO [2] and Takanari OGATA [3]

[1] *Argonne National Laboratory, 9700 S Cass Ave, Lemont, IL 60439, USA*
[2] *Japan Atomic Energy Agency, 4002 Narita, Oarai, Ibaraki, 311-1393, Japan*
[3] *Central Research Institute of Electric Power Industry, 2-6-1 Nagasaka, Yokosuka-shi, Kanagawa, 240-0196, Japan*

Assembly core bowing and core radial expansion are important features in sodium-cooled fast reactors due to the sensitivity of the reactivity feedbacks to small displacements of the active fuel in the core. These negative feedbacks are especially important during abnormal transients such as unprotected transient overpower and unprotected loss of flow. To characterize the negative feedback effects, accurate prediction of the fuel assembly displacement is important. The objective of this study is to increase confidence in the estimation of core duct bowing using multi-duct thermal bowing experiment data. Through a bilateral United States – Japan collaboration, ANL, JAEA, and CRIEPI performed thermal bowing analysis of their core bowing codes comparing the results to validation data of multi-duct thermal bowing and contact force measurements. Comparisons of the analysis results with the experimental measurements showed the core bowing codes were able to reasonably predict the assembly bowing displacement values and contact at the load pads.

KEYWORDS: core bowing, code validation, reactivity feedback, Joyo ex-core benchmark, SFR, radial core expansion

I. Introduction

Assembly core bowing is an important passive safety feature in sodium-cooled fast reactors. Reactivity changes can result from relatively small movement of fuel assemblies within the reactor core and can help contribute to a negative net reactivity during transient scenarios such as transient overpower and unprotected loss of flow. Core bowing is a Multiphysics phenomenon based on the interactions between neutronics, thermal-hydraulics, and structural mechanics. When multiple ducts are involved, the contact of the ducts presents a uniquely difficult challenge due to the highly non-linear nature of the contact development along the different contact planes between the ducts. To reduce uncertainties in the calculation of core bowing phenomenon, verification and validation efforts are important. Thus, an international framework for code-to-code verification and validation (V&V) has been developed based on a report by the International Working Group on Fast Reactors (IWGFR).[1,2] The report contained validation benchmarks for two single-duct thermal bowing experiments, one with restraints at the load pads and one with no restraints, and one multi-duct thermal bowing experiment with a row of 10 ducts, which were based on the Joyo ex-core thermal bowing experiments. To reliably consider uncertainties in the software analysis, Argonne National Laboratory (ANL), Central Research Institute of Electric Power Industry (CRIEPI), and Japan Atomic Energy Agency (JAEA) conducted a validation study of the Joyo ex-core experiments with their own respective duct bowing software and compared the results through a bilateral collaboration between the United States and Japan. The validation studies are divided into two parts: single-duct and multi-duct experiments. This paper describes the analysis results of the multi-duct experiments and expands on a companion study to model thermal bowing of single duct experiments.[3)]

*Corresponding author, E-mail: nwozniak@anl.gov

II. Multiple Duct Bowing Experiment

The test setup schematic is shown in **Fig. 1** and includes 10 Joyo-type fuel assembly ducts in a row inserted into a nozzle sleeve at the bottom core support plate with upper and lower pads on each side and individual heaters placed inside the ducts on one side to induce bowing from left to right due to differential thermal expansion of the duct. The bending stiffness of the fuel pin bundles is negligible compared with the ducts, so the bending deformation of the fuel assemblies is determined only by the ducts. Thus, this experimental focuses only on the thermal bowing deformation of the ducts. **Table 1** shows the nominal specifications of a single duct within the row of ducts. Each duct parameter, such as the duct across-flats dimensions, wall thicknesses, and load pad thicknesses were measured individually to account for the individual bending stiffness, gaps, and contact behavior between adjacent ducts. The row of ducts is restrained at the upper and lower pads at the SA0 and SA9 with load cell (LC) which limits the maximum amount of thermal bowing the

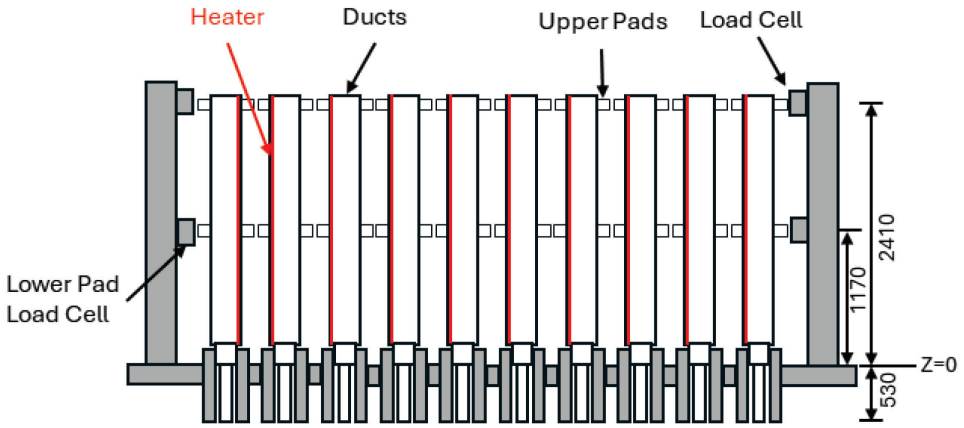

(Unit: mm)

Fig. 1 Multiple duct experiment setup

Table 1 Assembly duct nominal specifications

Position	Value
Duct total length (mm)	2970
Elevation of upper pad (mm)	2410
Elevation of lower pad (mm)	1170
Duct outer flat-to-flat (mm)	78.32
Duct wall thickness (mm)	1.45
Spring stiffness at upper pad	Rigid
Spring stiffness at lower pad (N/mm)	2.35×10^3
Clearance at entrance nozzle	0.15

ducts can reach before contact at the upper restraint occurs. The row of ducts simulates the central row of ducts within a reactor core, with the leftmost duct representing the center of the core, the middle ducts representing the active fuel assemblies, and the rightmost ducts representing the shield and reflector assemblies bowing into the restraint rings along the core barrel. In the experimental setup, the displacements were measured at 10 axial locations by a laser transit tracking a marking line on the outside of the ducts and the contact loads were measured at the outer ducts by load cells placed at the upper and lower restraints.

III. Analysis Codes for SFR Core Bowing

To simulate the duct thermal bowing and estimate the deflections and contact forces, ANL, JAEA, and CRIEPI, used independently developed codes to perform the analysis, NUBOW-3D,[4] FINAS,[5] and ARKAS,[6] respectively. For consistent modeling of the thermal bowing, contact at the load pads, and nozzle boundary condition, the analysis model in **Fig. 2** was developed and used for each code. The ducts were modeled along their entire length by beam elements with contact enforcement at the specific axial locations of the upper and lower load pads. The lower entrance nozzle was specifically modeled in NUBOW-3D and FINAS by considering a beam with the length of the nozzle restricting the translation displacement at the nozzle pivot point and leaving a small gap at the bottom of the nozzle consistent with the experimental setup. The ARKAS code does not model the nozzle explicitly but includes the equivalent rotational stiffness of the nozzle to simulate the same pivot support rotation.

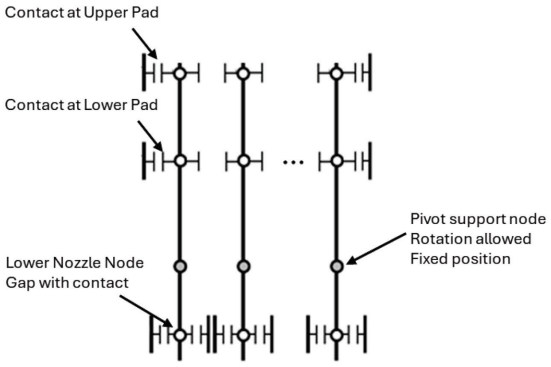

Fig. 2 Core bowing analysis model for multiple ducts

IV. Analysis Results and Discussion

The validation study consisted of six cases, labeled M1 to M6, of experimental test setups, each characterized by different initial gap widths at the restraint load pads and between each of the ducts, as well as different temperature gradients along the duct cross-sections. **Table 2** shows the initial gap widths at the upper and lower pads between all ducts and the restraints for each case. Initial gaps in M1 were relatively small with 1.07 mm at the upper pad and 0.88 mm at the lower pad between duct SA9 and the LC while M6 had no gap at the upper and lower pads between duct SA9 and the LC. Cases M2 – M3 and M4 – M5 had identical gaps between each other, but different temperature gradients. **Table 3** shows the temperature difference across the faces of each duct in case M2 at each of the different axial points where the temperatures were measured. Positive values for the difference indicate the temperature is greater on the left and induces duct bowing from left to right (positive bowing) while negative values for the difference indicate the temperature is greater on the right and induces duct bowing from right to left (negative bowing).

The bowing displacement results for the experimental measurements and analysis are shown in **Fig. 3** for all cases M1 – M6. In each experiment, horizontal displacements were measured at the axial positions of 570, 770, 970, 1170, 1370,

Table 2 Initial gap width (mm) at the upper and lower pads between ducts

Case	Position	LC – 0	0 – 1	1 – 2	2 – 3	3 – 4	4 – 5	5 – 6	6 – 7	7 – 8	8 – 9	9 – LC
M1	Upper	0.03	0.00	2.68	0.62	2.05	0.00	0.00	3.37	0.00	0.28	1.07
	Lower	0.00	0.00	0.00	0.00	0.00	0.23	0.00	0.35	0.20	0.00	0.88
M2	Upper	0.13	0.15	2.85	0.50	2.10	0.00	0.13	3.95	0.00	0.30	1.15
	Lower	0.00	0.00	0.00	0.00	0.00	0.35	0.00	0.47	0.23	0.00	0.94
M3	Upper	0.13	0.15	2.85	0.50	2.10	0.00	0.13	3.95	0.00	0.30	1.15
	Lower	0.00	0.00	0.00	0.00	0.00	0.35	0.00	0.47	0.23	0.00	0.94
M4	Upper	0.20	0.00	2.88	0.45	2.04	0.00	0.00	4.45	0.00	0.20	3.25
	Lower	0.00	0.00	0.00	0.00	0.00	0.33	0.00	0.53	0.20	0.00	0.00
M5	Upper	0.20	0.00	2.88	0.45	2.04	0.00	0.00	4.45	0.00	0.20	3.25
	Lower	0.00	0.00	0.00	0.00	0.00	0.33	0.00	0.53	0.20	0.00	0.00
M6	Upper	0.20	0.00	2.90	0.40	2.04	0.00	0.00	3.90	0.00	0.15	0.00
	Lower	0.00	0.00	0.00	0.00	0.00	0.30	0.00	0.31	0.13	0.00	0.00

Table 3 Temperature difference (°C) across the faces of each duct for case M2

Z (mm)	SA0	SA1	SA2	SA3	SA4	SA5	SA6	SA7	SA8	SA9
800	-9.0	15.5	14.4	16.7	19.3	16.4	16.5	23.4	25.7	0.0
1040	-9.0	10.1	15.7	18.0	25.0	18.3	14.9	20.1	28.2	0.3
1340	-9.0	7.5	18.0	17.5	19.8	20.8	18.0	20.6	24.4	0.0
1840	-7.7	10.8	14.6	19.6	16.7	14.1	19.0	17.7	23.2	0.3
2070	-	13.2	10.2	10.1	18.2	11.8	15.8	16.9	25.2	-
2310	-1.5	0.0	1.5	1.3	-0.5	0.0	-2.1	-1.7	1.8	3.6

1570, 1770, 1970, 2170, and 2370 mm from the core support plate. Based on the displacement plots, all three analysis codes were able to reasonably predict the direction and shape of the duct displacements. As the temperatures induce bowing displacement from left to right, the ducts deform towards the right restraint until contact occurs between SA9 and the LC at the restraint. Due to this contact behavior and the relatively large temperature difference between the outer ducts, (SA5 – SA8), displacement toward the left of the row of ducts (reverse bowing) occurs, enforcing contact at the lower pad and mimicking compaction at the lower pad. Each of the three codes was able to reproduce this behavior, with the largest differences occurring at ducts SA7 and SA8 for case M1, SA1 and SA3 for case M2, SA1 and SA3 for case M3, and SA0 and SA8 for case M6. A potential cause for those discrepancies, after factoring in displacement measurement precision, is the uncertainty of the individual value of the gap and the relative contact stiffness at both the upper and lower pad planes of the ducts. A lower value of the pad stiffness would allow larger estimation of the displacement during contact enforcement due to compression of the ducts and interpenetration of the beam nodes. Experimental results for cases M4 and M5 ducts SA0, SA1, and SA2 displayed an initial offset in all the displacement values which were inconsistent with the test setup; SA0 had an initial offset displacement of 4.75 mm. When considering the initial displacement and reducing all the displacement values by 4.75 mm, the displacement shape and trends for these three assemblies in both cases M4 and M5 match very well.

Table 4 shows the measured maximum displacement (D_{max}) for case M1 and the Mean Absolute Error (MAE) calculated from the analysis results and measurements:

$$MAE = \frac{1}{n}\sum_{i=1}^{n}|C_i - M_i| \quad (1)$$

where C is the calculated value, M is the measurement value, and n is the sample size. The MAEs for the ducts SA1 – SA6 were within 20% of D_{max} with the largest differences occurring near the top of the duct, which in a typical SFR design has no fuel pins and thus has a relatively small or negligible reactivity worth value. SA0 has the largest relative differences based on very small displacements.

Figure 4 shows the comparison of the calculated contact forces at the upper and lower pads between ducts SA0 and SA9 and the restraint load cells for all cases. **Table 5** shows the calculation of the relative error between the contact at SA0 and the upper load cell for all cases. The contact force calculation agreed within 40% except for case M5, which shows larger differences, while M6 agreed within 20%. The three codes were able to calculate contact interaction between the upper pad and restraint at SA9, despite the values showing differences. The largest differences were in estimating contact interaction at the lower pad between SA0 and the restraint. A potential cause for this behavior was noted with the displacements, regarding the contact stiffness of the ducts estimated as potentially low relative to the experimental setup. Another potential cause for the trends of disagreement between the experimental measurements and the analysis results can be due to the measurement uncertainty of the initial gaps between the ducts. Measurements of the initial gaps were

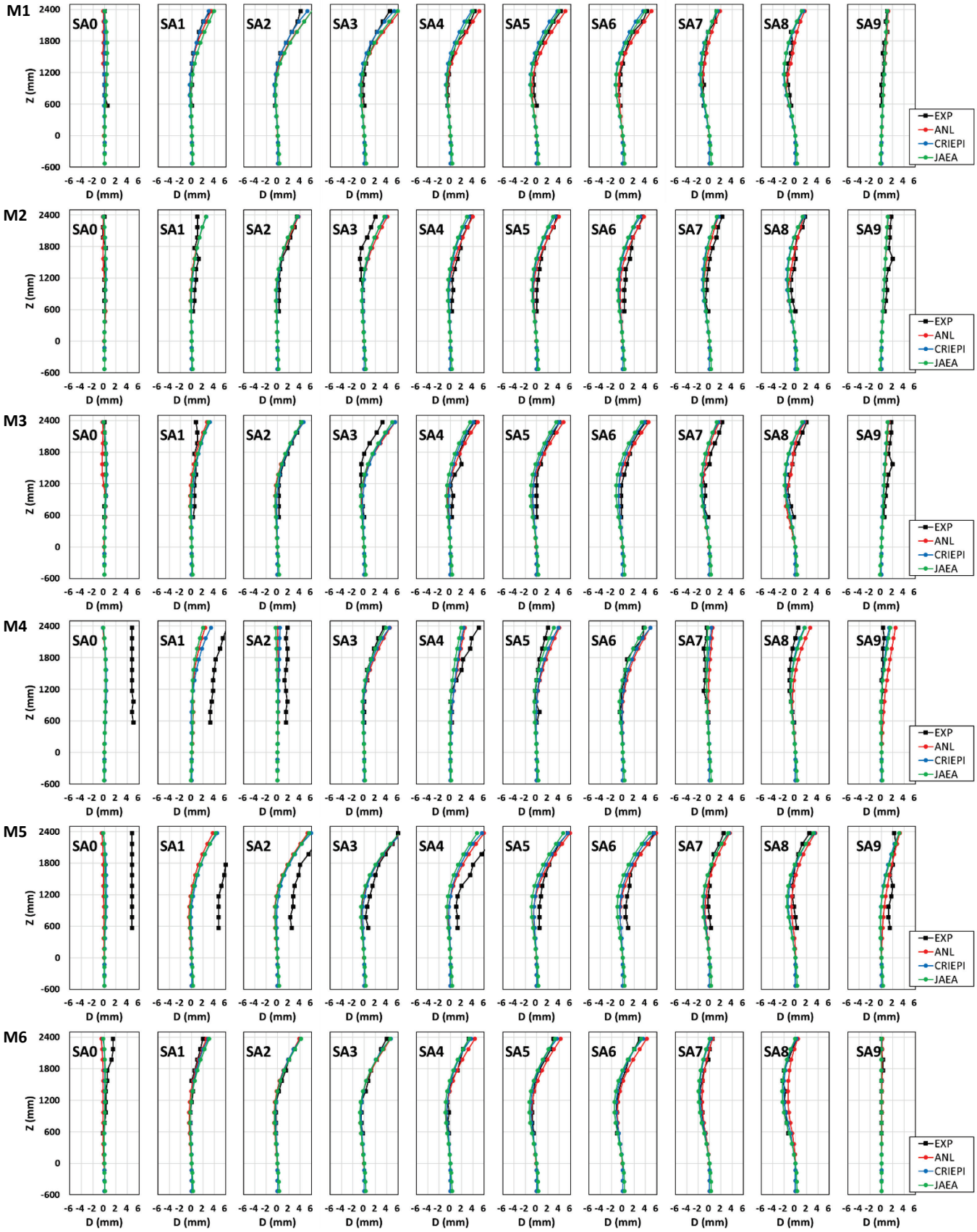

Fig. 3 Horizontal displacements (D) of each duct for cases M1 – M6

Table 4 Maximum horizontal displacement (D_{max}) and Mean Absolute Error for ducts in case M1

			SA0	SA1	SA2	SA3	SA4	SA5	SA6	SA7	SA8	SA9
Exp	D_{max}	(mm)	0.50	3.25	4.00	4.50	4.25	4.25	4.25	1.25	1.50	1.00
ANL	MAE	(mm)	0.20	0.21	0.55	0.68	0.28	0.50	0.32	0.25	0.42	0.27
	MAE/D_{max}	(%)	39	7	14	15	7	12	8	20	28	27
CRIEPI	MAE	(mm)	0.09	0.17	0.20	0.39	0.49	0.60	0.70	0.36	0.48	0.23
	MAE/D_{max}	(%)	19	5	5	9	11	14	17	29	32	23
JAEA	MAE	(mm)	0.30	0.48	0.65	0.55	0.28	0.39	0.52	0.27	0.44	0.21
	MAE/D_{max}	(%)	60	15	16	12	7	9	12	22	30	21

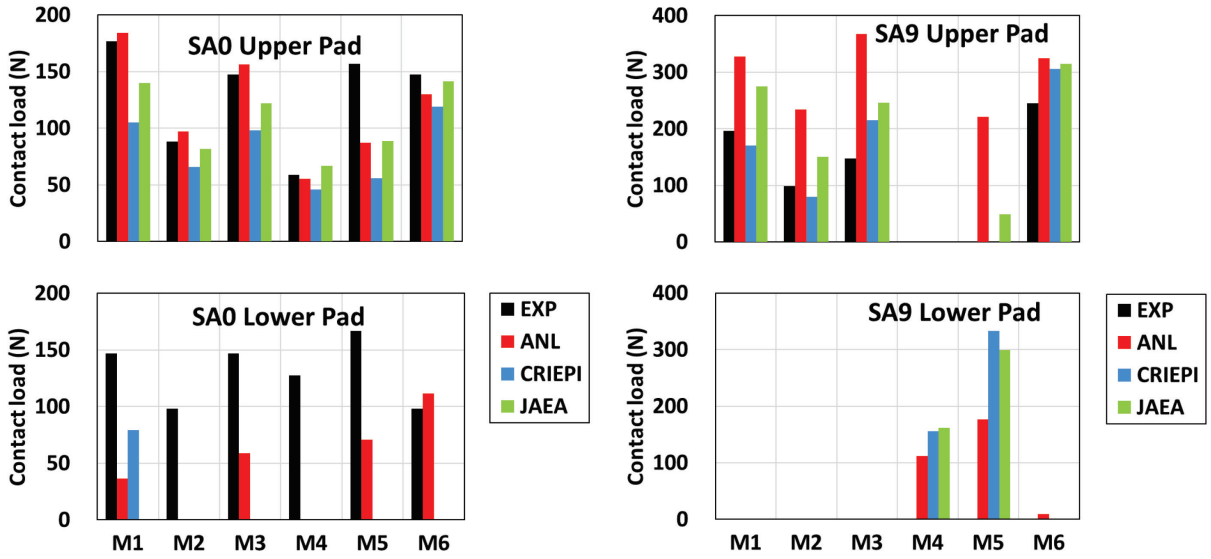

Fig. 4 Comparison of contact forces at the load pads

Table 5 Contact force (N) between the upper pad of SA0 and the restraint load cell

Case	M1		M2		M3		M4		M5		M6	
	(N)	(%)	(N)	(%)	(N)	(%)	(N)	(%)	(N)	(%)	(N)	(%)
Exp	176.5	-	88.3	-	147.1	-	58.8	-	156.9	-	147.1	-
ANL	184.0	4	97.2	10	156.0	6	55.2	-6	87.4	-44	130.0	-12
CRIEPI	105.0	-41	66.0	-25	98.0	-33	46.0	-22	56.0	-64	119.0	-19
JAEA	139.6	-21	81.5	-8	122.2	-17	67.0	14	88.7	-43	141.2	-4

conducted with a gap gauge, but there is no information on the precision or measurement uncertainty. The experimental setup and phenomenon pose many complexities and uncertainties in the analysis setup, and very slight differences in the values of the initial gaps and contact stiffness for the analysis could produce large discrepancies in the estimation of the bowing and contact forces, since the model contains multiple ducts with many gap and contact points between each duct. Despite those differences with the experimental measurements, the codes agreed reasonably well with each other, which provides confidence that the codes can reproduce core bowing displacements and contact behavior.

Due to the complex behavior of a row of multiple ducts bowing and contacting each other, coupled with large system and measurement uncertainties, this validation analysis warrants further investigation into the sensitivity of the results to system parameters, specifically the initial gaps at the restraints and between the ducts as well as the stiffness of the lower pad.

V. Conclusion

ANL, JAEA, and CRIEPI conducted a validation study of their respective core duct bowing analysis codes by using the fuel assembly design and thermal bowing measurements from the Joyo ex-core experiment and compared the results. For the multi-duct experiments, the analysis results of the three codes for the horizontal displacements and contact loads agreed with each other and reproduced the test results for most of the ducts in each case. Notable differences were the displacements of the ducts SA7 and SA8 for case M1, SA1 and SA3 for case M2, SA1 and SA3 for case M3, and SA0 and SA8 for case M6 as well as the contact forces at the lower pad. Initial offset displacement values were also highlighted for SA0, SA1 and

SA2 for cases M4 and M5 which were inconsistent with the experimental setup. The code validation study using the multi-duct experiments confirmed that the core bowing analysis codes were able to reasonably predict the thermal bowing trend and shape for a row of ducts, but further investigation into test uncertainties could shed light on the current discrepancies in the results, specifically the initial load pad gap values and their effect on the estimation of the contact forces.

Acknowledgment

Argonne's work was funded by the U.S. Department of Energy Office of Nuclear Energy's (DOE-NE) Fast Reactor Program (FRP).

The submitted manuscript has been created by UChicago Argonne, LLC, Operator of Argonne National Laboratory ("Argonne"). Argonne, a U.S. Department of Energy Office of Science laboratory, is operated under Contract No. DE-AC02-06CH11357. The U.S. government retains for itself, and others acting on its behalf, a paid-up nonexclusive, irrevocable worldwide license in said article to reproduce, prepare derivative works, distribute copies to the public, and perform publicly and display publicly, by or on behalf of the Government. The Department of Energy will provide public access to these results of federally sponsored research in accordance with the DOE Public Access Plan. http://energy.gov/downloads/doe-public-access-plan

JAEA's and CRIEPI's work includes some of the results of the "Technical development program on a fast reactor for demonstration (Program Grant Number JPMT007143)" ensured to JAEA by the Ministry of Economy, Trade and Industry in Japan (METI). The JAEA authors thank M. Iida of NESI Inc. for his assistance with the computational work.

References

1) International Atomic Energy Agency, "Verification and validation of LMFBR static core mechanics codes part I," IWGFR/75, 1990.
2) International Atomic Energy Agency, "Verification and validation of LMFBR static core mechanics codes part II," IWGFR/76, 1990.
3) Ohgama, K., Doda, N., Ohta, H., Wozniak, N., Uwaba, T., Futagami, S., Tanaka, M., Yamano, H., Ogata, T., Shemon, E., Feng, B., "Validation study on SFR core bowing codes using Joyo ex-core experiment data: single duct bowing benchmark," *Progress in Nuclear Science and Technology*, (submitted 2024).
4) G. A. McLennan, T. J. Moran, B. K. Cha, "Core structural analysis codes verification/qualification.[LMFBR]," *Trans. Am. Nucl. Soc.*, **30**, CONF-7811109- (1978).
5) K. Iwata, "General purpose nonlinear program FINAS for elevated temperature design of FBR components," *ASME Pressure Vessel and Piping Conference*, **66**, 119-137 (1982).
6) M. Nakagawa, "ARKAS: A three-dimensional finite element program for the core-wide mechanical analysis of liquid-metal fast breeder reactor cores," *Nuclear Technology*, **75**[1], 46-65 (1986).